

From inflation to cosmological electroweak phase transition with a complex scalar singlet

Wei Cheng¹ and Ligong Bian^{1,2,*}

¹*Department of Physics, Chongqing University, Chongqing 401331, China*

²*Department of Physics, Chung-Ang University, Seoul 06974, Korea*



(Received 8 January 2018; published 18 July 2018)

We investigate the possibility of addressing inflation, a strongly first-order electroweak phase transition (SFOEWPT) together with the dark matter (DM) explanation simultaneously. We study the Higgs-portal real scalar singlet model and the complex scalar singlet model. In both models, the SFOEWPT can occur through two-step patterns in which the magnitude of the Higgs-singlet quartic couplings meets the slow-roll condition of inflation. The Higgs-portal real scalar singlet model cannot address the correct DM relic density together with the explanation of inflation and SFOEWPT. Taking advantage of the cancellation in the DM-nucleon interaction, the weakly interacting massive particles DM can saturate the correct DM relic abundance in the complex scalar singlet model, with the pseudoscalar being the DM candidate after the global U(1) symmetry is broken. The key ingredient in obtaining the successful inflation and the SFOEWPT is that the magnitude of the scalar quartic couplings should be relatively lower. Because the cancellation of the DM-nucleon scattering amplitude mediated by mixtures of SM Higgs and other heavy scalars can occur to a different extent in many models, we can expect that the features being explored here are general.

DOI: [10.1103/PhysRevD.98.023524](https://doi.org/10.1103/PhysRevD.98.023524)

I. INTRODUCTION

Up to now, the standard model of particle physics (SM) describes three fundamental interactions in nature fairly well. Unfortunately, the incompleteness of the SM makes it fail when confronting the three long-standing particle physics and cosmology problems, i.e., the horizon and flatness problems of the Universe, the baryon asymmetry of the Universe, and the existence of the dark matter. First, cosmic inflation successfully solves the first problem [1–3] and explains the large-scale structure of the Universe observed by the cosmic microwave background (CMB) [4] with the primordial fluctuations. The observation of the SM Higgs at LHC [5,6] make the Higgs inflation [7,8] more predictive and standing out from variants of cosmic inflation mechanisms. While the original Higgs inflation is beset by the unitarity problem at a high scale around $\sim \mathcal{O}(10^{13})$ GeV induced by the Higgs-gravity nonminimal coupling [9–19], which requires the Higgs sectors of the SM to be extended, one of the most economic ways can be the “Higgs portal” [20,21]. Second, the SM is incapable of explaining the baryon asymmetry of the Universe (BAU)

because the Sakharov conditions [22] cannot be fulfilled; i.e., the CP source coming from the Cabibbo-Kobayashi-Maskawa matrix is insufficient, and the strongly first-order electroweak phase transition (SFOEWPT) suppressing the baryon asymmetry washout process is unreachable because of the overlarge magnitude of the Higgs mass [23].¹ The mechanism of electroweak baryogenesis (EWBG) can solve the puzzle of the BAU with a SFOEWPT occurs at the electroweak scale, followed by the electroweak symmetry breaking [23]. As requested by the SFOEWPT, the Higgs sectors of the SM, which can be tested at high-energy colliders through the detection of the deviations of the triple Higgs couplings, need to be extended [25]. For the study of EWBG with the simple singlet scalar extended SM, see Refs. [26,27] for the real scalar singlet case and Refs. [28,29] for the complex scalar singlet case. Another shortcoming of the SM is the absence of the DM candidate, which is supported by overwhelming well-established astrophysical and cosmological observations. One of the simplest solutions is to extend the scalar sectors and employ the Higgs-portal approach to gain the weakly interacting massive particles (WIMPs) DM [30]. At present, with the accumulation of indirect and direct detection experimental data of DM, the WIMPs DM is under increasing pressure. The parameter spaces of the simplest Higgs-portal scalar dark matter model are almost

*lgbycl@cqu.edu.cn

Published by the American Physical Society under the terms of the Creative Commons Attribution 4.0 International license. Further distribution of this work must maintain attribution to the author(s) and the published article's title, journal citation, and DOI. Funded by SCOAP³.

¹The phase transition in the SM is in fact the crossover pattern; a SFOEWPT requires a Higgs mass around 70–80 GeV [23,24].

excluded [31–33] except the *Higgs funnel regime* $m_{\text{DM}} \sim m_h/2$. Fortunately, in the simplest complex scalar singlet model, see Refs. [34–37], the global $U(1)$ symmetry can be broken, and the pseudoscalar serves as the WIMPs DM candidate. Therein, the cancellation in the DM-nucleon scattering process happens due to the mixing of the real part of the singlet and the SM-like Higgs, as highlighted in Ref. [38], which can save a lot of WIMPs DM parameter spaces from the ongoing direct detection experiments bounds.

We investigate the possibility of implementing the paradigms of inflation, the SFOEWPT, and WIMPs DM simultaneously by means of extending the SM with a complex scalar singlet. The cancellation of the Higgs mixtures mediated DM-SM particle scattering amplitude makes the pseudoscalar able to saturate the DM at any mass regions avoiding the constraints from ongoing direct detection experiments. To satisfy the slow-roll condition of the Higgs/singlet inflation, the quartic scalar couplings is found to be small, and a SFOEWPT occurs as the temperature cools down. Supplemented by an additional CP -violation source, the successful inflation, EWBG, and correct DM relic density can be reached simultaneously in certain parameter spaces of the singlet scalar vacuum expectation value (VEV) and heavy Higgs masses. The model is described in Sec. II, in which the real scalar singlet model can be obtained when the global $U(1)$ is reduced to Z_2 symmetry. The ingredients for cosmic inflation, SFOEWPT, and dark matter in the model are given in Sec. III. The numerical results of the whole physical pictures of the three components are accomplished in Sec. IV. We conclude in Sec. V.

II. MODEL

In this work, we employ a complex scalar singlet model with the tree-level potential being given by

$$V_0(H, \mathcal{S}) = -\mu_h^2 |H|^2 + \lambda_h |H|^4 - \mu_s^2 |\mathcal{S}|^2 + \lambda_{hs} |H|^2 |\mathcal{S}|^2 + \lambda_s |\mathcal{S}|^4 - \left(\frac{1}{2} \mu_b^2 \mathcal{S}^2 + \text{H.c.} \right). \quad (1)$$

A real mass term μ_b is introduced to break the global $U(1)$ $\mathcal{S} \rightarrow e^{i\alpha} \mathcal{S}$ symmetry, which makes the imaginary parts of \mathcal{S} serve as a DM candidate. After inserting the scalar field configurations $H^T = (0, h)/\sqrt{2}$ and $\mathcal{S} = (s + iA)/\sqrt{2}$, we obtain

$$V_0(h, s, A) = \frac{\lambda_h h^4}{4} + \frac{1}{4} \lambda_{hs} h^2 A^2 - \frac{\mu_h^2 h^2}{2} + \frac{1}{4} \lambda_{hs} h^2 s^2 + \frac{\lambda_s A^4}{4} - \frac{\mu_s^2 A^2}{2} + \frac{\mu_b^2 A^2}{2} + \frac{\lambda_s s^4}{4} + \frac{1}{2} \lambda_s s^2 A^2 - \frac{\mu_s^2 s^2}{2} - \frac{\mu_b^2 s^2}{2}. \quad (2)$$

The vacuum stability requires the tree-level potential to be bounded from below,

$$\lambda_h > 0, \quad \lambda_s > 0, \quad \lambda_{hs} > -2\sqrt{\lambda_h \lambda_s}. \quad (3)$$

The minimization conditions of the potential are

$$\left. \frac{dV_0(h, s, A)}{dh} \right|_{h=v} = 0, \quad \left. \frac{dV_0(h, s, A)}{ds} \right|_{s=v_s} = 0, \quad (4)$$

which give rise to

$$\begin{aligned} \mu_h^2 &= \lambda_h v^2 + \lambda_{hs} v_s^2/2, \\ \mu_s^2 &= -\mu_b^2 + \lambda_{hs} v^2/2 + \lambda_s v_s^2. \end{aligned} \quad (5)$$

The pseudoscalar DM mass is given by $m_A = \mu_b$. The mass matrix of the real scalars is given by

$$\mathcal{M}^2 = \begin{pmatrix} 2v^2 \lambda_h & v v_s \lambda_{hs} \\ v v_s \lambda_{hs} & 2v_s^2 \lambda_s \end{pmatrix}. \quad (6)$$

To diagonalize the mass matrix, we introduce the rotation matrix $R = ((\cos \theta, \sin \theta), (-\sin \theta, \cos \theta))$ with $\tan 2\theta = -\lambda_{hs} v v_s / (\lambda_h v^2 - \lambda_s v_s^2)$ to relate the mass basis and field basis,

$$\begin{pmatrix} h_1 \\ h_2 \end{pmatrix} = \begin{pmatrix} \cos \theta & \sin \theta \\ -\sin \theta & \cos \theta \end{pmatrix} \begin{pmatrix} h \\ s \end{pmatrix}. \quad (7)$$

The mass-squared eigenvalues are obtained as

$$m_{h_1, h_2}^2 = \lambda_h v^2 + \lambda_s v_s^2 \mp \frac{\lambda_s v_s^2 - \lambda_h v^2}{\cos 2\theta}. \quad (8)$$

We identify the h_1 as the 126 GeV SM-like Higgs boson and require the h_2 to be dominated by s in this work. The quartic couplings can be expressed as functions of the Higgs masses, v , v_s , and the mixing angle θ ,

$$\lambda_h = \frac{\cos(2\theta)(m_{h_1}^2 - m_{h_2}^2) + m_{h_1}^2 + m_{h_2}^2}{4v^2}, \quad (9)$$

$$\lambda_s = \frac{\cos(2\theta)(m_{h_2}^2 - m_{h_1}^2) + m_{h_1}^2 + m_{h_2}^2}{4v_s^2}, \quad (10)$$

$$\lambda_{hs} = \frac{\tan(2\theta) \cos(2\theta)(m_{h_2}^2 - m_{h_1}^2)}{2v v_s}. \quad (11)$$

The mixing angle and the heavy Higgs masses are sub-jetive to the bounds coming from the LHC Higgs data. The mixing of the h and s may lead to T parameter violation, which sets stringent bounds on the mixing angle and the masses of the heavy Higgs. One can obtain the oblique parameter T with the formula of

$$T = -\left(\frac{3}{16\pi s_W^2}\right) \left\{ \cos^2\theta \left[\frac{1}{c_W^2} \left(\frac{m_{h_1}^2}{m_{h_1}^2 - M_Z^2} \right) \ln \frac{m_{h_1}^2}{M_Z^2} - \left(\frac{m_{h_1}^2}{m_{h_1}^2 - M_W^2} \right) \ln \frac{m_{h_1}^2}{M_W^2} \right] + \sin^2\theta \left[\frac{1}{c_W^2} \left(\frac{m_{h_2}^2}{m_{h_2}^2 - M_Z^2} \right) \ln \frac{m_{h_2}^2}{M_Z^2} - \left(\frac{m_{h_2}^2}{m_{h_2}^2 - M_W^2} \right) \ln \frac{m_{h_2}^2}{M_W^2} \right] \right\}, \quad (12)$$

following the Feynman diagram method in Ref. [39]. The SM T parameter T^{SM} can be recovered when $\cos\theta = 1$. The quantity $\Delta T = T - T^{\text{SM}}$ is subjected to the bound coming from the current global electroweak (EW) fit [40]: $\Delta T = 0.09 \pm 0.13$. One can obtain severe constraints on the θ with the increasing of m_{h_2} . Recent combined analysis of the LHC Higgs data and the electroweak precision observables performed by Refs. [27,41] suggest the mixing angle θ can be as large as 0.2 for a moderate heavy Higgs mass.

The model has been extensively studied to explain one or two of the inflation, electroweak phase transition (EWPT), and DM; see Ref. [38] for a recent DM study, Ref. [42] for the studies of both inflation and the EWPT, and Refs. [28,29,36,37] for the study of the EWPT and DM. In this work, we explore the three of the inflation, EWPT, and DM. When the U(1) is reduced to Z_2 with the pseudoscalar and U(1) breaking term being absent with $\mu_b = 0$, the model reduces to the usual Higgs-portal real scalar singlet DM model, in which the s field can serve as the DM candidate and make the realization of slow-roll inflation [42] possible. In this case, the DM mass m_s is easy to obtain from Eqs. (2) and (4) with $A = 0$ and $v_s = 0$, $m_s^2 = -\mu_s^2 + \lambda_{hs}v^2/2$, where μ_s^2 can be positive or negative, provided the EW vacuum is the global vacuum. As studied in previous literature, see Refs. [43,44], it is easier for a positive μ_s^2 to let the two-step phase transition occur, which allows a local minimum at $(h, s) = (0, \pm\sqrt{\mu_s^2/\lambda_s})$ to coexist with the global EW vacuum. Recently, the possibility of implementing the SFOEWPT together with DM has been explored by Ref. [45]. Reference [46] studied the possibility of realizing the slow-roll inflation, SFOEWPT, and DM explanation in the model with typical DM masses of m_s . In this work, we explore the possibility of accomplishing the three within the two-step phase transition favored parameter spaces.

III. INGREDIENTS OF INFLATION, PHASE TRANSITION, AND DARK MATTER

For comparison and completeness, we include the inflation, EWPT, and DM phenomenology studies in both the Higgs-portal real scalar singlet DM and the complex scalar singlet model. In this section, we present the approach we employed to perform the numerical analysis of the three components.

A. Scalar portal inflation dynamics

For the slow-roll inflation dynamics analysis, we follow the approach of Refs. [42,47]. In the U(1) complex scalar singlet model, the action in the Jordan frame is

$$S_J = \int d^4x \sqrt{-g} \left[-\frac{M_{\text{P}}^2}{2} R - \xi_h (H^\dagger H) R - \xi_s (S^\dagger S) R + \partial_\mu H^\dagger \partial^\mu H + \partial_\mu S^\dagger \partial^\mu S - V(H, S) \right], \quad (13)$$

where M_{P} is the reduced Planck mass, R is the Ricci scalar, and $\xi_{h,s}$ define the nonminimal coupling of the h, s field.

The quantum-corrected effective Jordan frame Higgs potential at large field values $[h(s)]$ can be written as

$$V(h(s)) = \frac{1}{4} \lambda_{h(s)}(\mu) h(s)^4, \quad (14)$$

along the two-field potential evaluated along the Higgs or singlet axis, where the scale can be defined to be $\mu \sim \mathcal{O}(h) \approx h$ in order to suppress the quantum correction. And the quartic couplings $\lambda_{h(s)}$ at the Planck scale can be obtained using the renormalization group equations given in Appendix B. We impose quantum corrections to the potential and calculate the quantum corrections in the Jordan frame before performing the conformal transformation as in Refs. [48,49]. After the conformal transformation,

$$\tilde{g}_{\mu\nu} = \Omega^2 g_{\mu\nu}, \quad \Omega^2 \equiv 1 + \frac{\xi_s s^2}{M_{\text{P}}^2} + \frac{\xi_h h^2}{M_{\text{P}}^2}, \quad (15)$$

and a field redefinition,

$$\frac{d\chi_h}{dh} = \sqrt{\frac{\Omega^2 + 6\xi_h^2 h^2/M_{\text{P}}^2}{\Omega^4}}, \quad \frac{d\chi_s}{ds} = \sqrt{\frac{\Omega^2 + 6\xi_s^2 s^2/M_{\text{P}}^2}{\Omega^4}}, \quad (16)$$

we obtain

$$S_E = \int d^4x \sqrt{-\tilde{g}} \left(-\frac{1}{2} M_{\text{P}}^2 R + \frac{1}{2} \partial_\mu \chi_h \partial^\mu \chi_h + \frac{1}{2} \partial_\mu \chi_s \partial^\mu \chi_s + f(\chi_s, \chi_h) \partial_\mu \chi_h \partial^\mu \chi_s - U(\chi_s, \chi_h) \right), \quad (17)$$

where $U(\chi_s, \chi_h) = \Omega^{-4} V(s(\chi_s), h(\chi_h))$ and

$$f(\chi_s, \chi_h) = \frac{6\xi_h \xi_s}{M_{\text{P}}^2 \Omega^4} \frac{ds}{d\chi_s} \frac{dh}{d\chi_h} h s. \quad (18)$$

Basically, we can obtain h and s inflations depending on if $\lambda_h/\xi_h^2 \ll \lambda_s/\xi_s^2$ or $\lambda_h/\xi_h^2 \gg \lambda_s/\xi_s^2$; see Refs. [42,47]. Then, the kinetic terms of the scalar fields are canonical.

We get the Einstein frame by locally rescaling the metric by a factor $\Omega^2 = 1 + (\xi_h h^2 + \xi_s s^2)/M_{\text{pl}}^2 \approx 1 + \xi_h h^2(s^2)/M_{\text{pl}}^2$ with $s(h) \sim 0$. The noncanonical kinetic term for h can be resolved by rewriting the inflationary action in terms of the canonically normalized field χ as

$$S_{\text{inf}} = \int d^4x \sqrt{\bar{g}} \left[\frac{M_{\text{p}}^2}{2} R + \frac{1}{2} (\partial\chi)^2 - U(\chi) \right], \quad (19)$$

with the potential in terms of the canonically normalized field χ as

$$U(\chi) = \frac{\lambda_h (h(\chi))^4}{4\Omega^4} \quad \text{or} \quad U(\chi) = \frac{\lambda_s (s(\chi))^4}{4\Omega^4}, \quad (20)$$

where the new field χ is defined by

$$\frac{d\chi}{dh} \approx \sqrt{(1 + \xi_h h^2/M_{\text{p}}^2 + 6\xi_h^2 h^2/M_{\text{p}}^2)/(1 + \xi_h h^2/M_{\text{p}}^2)^2} \quad (21)$$

or

$$\frac{d\chi}{ds} \approx \sqrt{(1 + \xi_s s^2/M_{\text{pl}}^2 + 6\xi_s^2 s^2/M_{\text{pl}}^2)/(1 + \xi_s s^2/M_{\text{pl}}^2)^2} \quad (22)$$

for h or s inflations [42]. Note that $\lambda_{h,s}$ and $\xi_{h,s}$ have a scale [$h(s)$] dependence.

The slow-roll parameters are then given by

$$\epsilon(\chi) = \frac{M_{\text{p}}^2}{2} \left(\frac{dU/d\chi}{U(\chi)} \right)^2, \quad \eta(\chi) = M_{\text{p}}^2 \left(\frac{d^2U/d\chi^2}{U(\chi)} \right). \quad (23)$$

The field value at the end of inflation χ_{end} is obtained when $\epsilon = 1$, and the horizon exit value χ_{in} can be calculated with a fixed e -folding number between the two periods,

$$N_e = \int_{\chi_{\text{end}}}^{\chi_{\text{in}}} d\chi \frac{1}{M_{\text{p}} \sqrt{2\epsilon}}. \quad (24)$$

Therefore, one can calculate the inflationary observables n_s and r with the slow-roll parameters at the χ_{in} ,

$$n_s = 1 + 2\eta - 6\epsilon, \quad r = 16\epsilon. \quad (25)$$

Meanwhile, the amplitude of scalar fluctuations $\Delta_{\mathcal{R}}^2$ can be calculated as

$$\Delta_{\mathcal{R}}^2 = \frac{1}{24\pi^2 M_{\text{p}}^4} \frac{U(\chi)}{\epsilon} = 2.2 \times 10^{-9}. \quad (26)$$

The CMB observation of the amplitude of scalar fluctuations [4] is used to determine $\xi_{h,s}$.² We use the Planck bounds [4] to require the values of n_s and r to be $n_s = 0.9677 \pm 0.0060$ at 1σ level and $r < 0.11$ at 95% confidence level by assuming $N_e = 60$, with which one can obtain the slow-roll inflation favored parameter regions of $\lambda_{h(s)}$ for Higgs (singlet) inflation, together with the Higgs-singlet quartic couplings λ_{hs} which contribute to the inflation potential through the renormalization group equations (RGEs) evolution effects as shown in Appendix A. In the complex scalar singlet case, these constraints transfer to the bounds on m_{h_2} , v_s , and the mixing angle of θ through Eq. (9). The slow-roll parameters r are typically of order $\sim \mathcal{O}(10^{-2})$ for our cases. The stability of the inflationary potential has been required by requiring conditions shown by Eq. (3) from the electroweak scale to the Planck scale using RGEs listed in Appendix A. The perturbativity of quartic coupling in the potential is also required as in Ref. [47], i.e., $|\lambda_h| < 1$, $|\lambda_{hs}| < \sqrt{4\pi}$, $|\lambda_s| < \sqrt{4\pi}$. As studied previously in Refs. [42,47], the successful implementation of slow-roll Higgs or singlet inflation requires a relatively lower magnitude of quartic scalar couplings, that prefer the two-step SFOEWPT, as will be explored in the next section.

The parametric resonance of the oscillating Higgs field to W bosons (singlet scalar) via $|H|^2|W|^2(|H|^2|S|^2)$ can help the Higgs (singlet) inflation reheating occur [42,51]. Reference [46] studied typical small $\lambda_s \sim \mathcal{O}(10^{-9} - 10^{-2})$ for singlet inflation reheating. Reference [21] studied s -inflation reheating with a larger λ_s , which can apply to our analysis. The reheating can happen through the stochastic resonance to the Higgs bosons or the production of the s -inflaton excitations in the case of the complex scalar singlet model, while for the Higgs-portal real scalar singlet DM model, the reheating can occur due to the production of the s -inflaton excitations in which $\lambda_s > 0.019$. After reheating, the Universe can undergo a cosmological phase transition at around the temperature of $T_C \sim \mathcal{O}(10^2)$ GeV, which we evaluate with the approach given in the following section.

B. Cosmological phase transition calculation approach

With the temperature cooling down, the Universe can evolve from the symmetric phase to the symmetry broken phase. The behavior can be studied with the finite temperature effective potential with particle physics models [52], through which one can obtain the critical classic field

²The nonminimal coupling for single-field inflation is generally of order $\mathcal{O}(10^4)$, which might lead to possible unitarity problems at a high scale around $\sim \mathcal{O}(10^{13})$ GeV [9–14], while Refs. [15–19] argued that the SM Higgs inflation do not necessarily involve the problem. The studies of Refs. [15,50] indicate that the perturbative unitarity breaking can be healed by the additional singlet. In this work, we do not address the issue.

value and temperature being v_C and T_C to characterize the critical phases. Roughly speaking, a SFOEWPT can be obtained when $v_C/T_C > 1$; then, the electroweak sphaleron process is quenched inside the bubble, and therefore one can obtain the net number of baryons over antibaryons in the framework of EWBG. For the uncertainty of the value and possible gauge-dependent issues, we refer to Ref. [53].

The effective potential includes the tree-level Higgs potential described by Eq. (2), the Coleman-Weinberg potential, and the finite temperature corrections take the form of [54]

$$V(h, s, A, T) = V_0(h, s, A) + V_{CW}(h, s, A) + V_{ct}(h, s, A) \\ + V_1(h, s, A, T) + V_{\text{daisy}}(h, s, A, T). \quad (27)$$

With the field-dependent masses being given in Appendix B, the one-loop Coleman-Weinberg scalar potential in $\overline{\text{MS}}$ and Landau gauge is

$$V_{CW}(h, s, A) = \frac{n_i}{4(4\pi)^2} M_i^4(h, s, A) \left(\log \frac{M_i^2(h, s, A)}{Q^2} - c_i \right), \quad (28)$$

with M_i to identify eigenvalues of the scalar matrix, and other field-dependent masses, here, $n_{h_1, h_2, h_3, G^\pm, G^0, W^\pm, Z, t} = 1, 1, 1, 2, 1, 6, 3, -12$, and $c_{W^\pm, Z} = 5/6$ with others c_i being $3/2$. The running scale Q is chosen to be $Q = 246.22$ GeV in the numerical analysis. The counterterms that can prevent the VEV shift by the one-loop Coleman-Weinberg potential are implemented following the approach of Ref. [55]. The finite temperature corrections to the effective potential at one loop are given by [52]³

$$V_1(h, s, A, T) = \frac{T^4}{2\pi^2} \sum_i n_i J_{B,F} \left(\frac{M_i^2(h, s, A)}{T^2} \right), \quad (29)$$

where the functions $J_{B,F}(y)$ are

$$J_{B,F}(y) = \pm \int_0^\infty dx x^2 \ln [1 \mp \exp(-\sqrt{x^2 + y})], \quad (30)$$

with the upper (lower) sign corresponding to bosonic (fermionic) contributions. Here, the above integral $J_{B,F}$ can be expressed as a sum of the second kind of modified Bessel functions $K_2(x)$ [55,56],

$$J_{B,F}(y) = \lim_{N \rightarrow +\infty} \mp \sum_{l=1}^N \frac{(\pm 1)^l y}{l^2} K_2(\sqrt{y}l). \quad (31)$$

Last but not least, the resummation of *ring* (or *daisy*) diagrams are also crucial for the evaluation of v_C and T_C with the finite temperature effective potential [57],

³The counterterms that can prevent the VEV shift by the one-loop Coleman-Weinberg potential are implemented implicitly following Ref. [55].

$$V_{\text{daisy}}(h, s, A, T) = \frac{T}{12\pi} \sum_i n_i [(M_i^2(h, s, A))^{3/2} \\ - (M_i^2(h, s, A, T))^{3/2}], \quad (32)$$

where $M_i^2(h, s, A, T)$ are the eigenvalues of the full bosonic mass matrix with thermal corrected effects being taken into account [$M_i^2(h, s, A, T) = M_i^2(h, s, A) + M_x^2(T)$]; the thermal correction masses $M_x^2(T)$ are given in Appendix B.

Then, the critical parameters of the SFOEWPT can be calculated when there are two degenerate vacuums with a potential barrier. Because of the rich vacuum structures of the potential at finite temperature, there can be one-step or multistep phase transitions. A SFOEWPT can be realized at the first or the second step in the two-step scenario. When the U(1) reduces to Z_2 symmetry with the pseudoscalar A absent, one returns to the usual real scalar singlet case. As studied previously in Ref. [45], a one-step SFOEWPT calls for a larger quartic coupling between h and s , while a two-step SFOEWPT can happen at a relatively smaller quartic coupling between h and s . When the singlet s serves as the DM candidate, the two-step mode indicates the Z_2 symmetry is broken at some higher finite temperatures and restored at some lower and zero temperatures [31,58]. In this case, the phase transition types occur as shown by the left panel of Fig. 1; the form of the finite temperature effective potential reduces from Eq. (27) to $V(h, s, T)$ without A contributions. At the critical temperatures for a different set of quartic couplings and dark matter masses, one has two local minima, wherein

$$V(0, s_C^A, T_C) = V(v_C^B, 0, T_C), \\ \left. \frac{dV(0, s, T_C)}{ds} \right|_{s=s_C^A} = 0, \\ \left. \frac{dV(h, 0, T_C)}{dh} \right|_{h=v_C^B} = 0. \quad (33)$$

For the phase transition to occur in this pattern, at zero temperature, the local vacuum in the direction of s [localized at $(h = 0, s = \pm \sqrt{\mu_s^2/\lambda_s})$] should be higher than the global electroweak vacuum at $(h = v, s = 0)$, which requires $\lambda_s > 2(m_s^2 - \lambda_{hs}v^2)/(m_h^2v^2)$. And the vacuum in the direction of s should appear earlier than that of the h with the temperature decreasing. As will be shown in Sec. IV, the two ingredients lead to the successful inflation in a tiny corner of parameter spaces where one can obtain a SFOEWPT in this model.

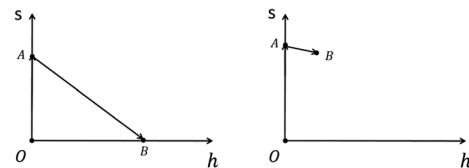


FIG. 1. EWPT types in the real scalar singlet and U(1) breaking complex scalar singlet models for the left and right panels.

For the complex singlet case, the studies of Refs. [28,29] show that the dark matter mass effects on the evolution of the effective potential with temperature cooling down is negligible. And for simplicity, we do not expect the A field get a VEV at finite temperature and focus on the case in which the vacua can happen along the h and/or s direction(s) with the temperature decreasing. As studied previously in Refs. [42,47], a relatively larger quartic scalar coupling will lead to the violation of the perturbativity and unitarity that will invalidate the slow-roll inflation. To obtain a strongly first-order phase transition together with the successful inflation, we focus on the two-step phase transition here. The right panel of Fig. 1 is for the phase transition type of the complex singlet case. Considering the mixing of h and s at zero temperature as shown in the Sec. II, the critical temperature and critical field value can be evaluated through

$$\begin{aligned} V(0, s_C^A, \theta, 0, T_C) &= V(v_C^B, s_C^B, \theta, 0, T_C), \\ \left. \frac{dV(h, s, \theta, 0, T_C)}{ds} \right|_{h=v_C^B, s=s_C^B} &= 0, \\ \left. \frac{dV(0, s, \theta, 0, T_C)}{ds} \right|_{s=s_C^A} &= 0, \end{aligned} \quad (34)$$

when two degenerate vacua with a potential barrier structure show up for a set of $m_{h_1, h_2, A}$ and θ at finite temperatures. We assume the classical field A does not get a VEV at any temperature, as mentioned before. Here, we note that, to ensure the phase transition occurs in this pattern, at zero temperature, the vacuum at $(h = 0, s^A = \pm\sqrt{\mu_s^2/\lambda_s})$ should be higher than the global vacuum at $(h = \pm\sqrt{(4\lambda_s\mu_h^2 - 2\lambda_{hs}\mu_s^2)/(4\lambda_h\lambda_s - \lambda_{hs}^2)}, s^B = \pm\sqrt{(4\lambda_h\mu_s^2 - 2\lambda_{hs}\mu_h^2)/(4\lambda_h\lambda_s - \lambda_{hs}^2)})$ [which is (v_h, v_s) of Sec. II]. The counterterm in Eq. (27) keeps the s_C^A and s_C^B around the s^A and s^B , respectively. A study of this pattern phase transition triggered by vector dark matter can be found in Ref. [59], in which a gauge-invariant approach is employed.

C. Dark matter

As noted by Ref. [60], when the freeze-out temperature (T_{fs}) is smaller than the EWPT temperature, the thermal averaged annihilation cross section [see Eqs. (C2–C10)] in the relic density evaluation process can be temperature independent. In particular, in the dark matter mass regions smaller than $\sim\mathcal{O}(10)$ TeV, one can always have $T_{fs} \leq T_C$. Therefore, one can calculate the relic density self-consistently in those dark matter mass regions. Furthermore, at this stage, the nonminimal gravity couplings' effect is negligible, and for the typical case of dark matter decay through the nonminimal gravity couplings, we refer to Refs. [61,62].

The thermal averaged dark matter pair annihilation cross sections are given by

$$\sigma v_r = \langle\sigma v\rangle_{ZZ} + \langle\sigma v\rangle_{WW} + \langle\sigma v\rangle_{f\bar{f}} + \langle\sigma v\rangle_{h_i h_j}, \quad (35)$$

with $i, j = 1, 2$, and these contributions are listed in Appendix C; these formulas simply reduce to the formula of Ref. [42] for the real scalar singlet case, which gives rise to the usual Higgs-portal real scalar singlet DM scenario. With the thermal averaged dark matter annihilation cross sections at hand, we calculate the relic density with the method of Ref. [63], which is checked to be around the percent level discrepancy with MICROMEAS [64]. The current value of the relic abundance of dark matter $\Omega_{dm} h^2 \approx 0.12$ [65]. Because of the mixing of h and s , one can expect the $h_{1,2}$ -mediated diagrams to contribute to the spin-independent cross section. Here, one notes that cancellation between the two parts of the scattering cross section can happen, as explored in Ref. [38]. The property would relax the parameter spaces being bounded by the direct detection experiments, especially after the strongest bounds coming from XENON1T [66].

IV. RESULTS

For the real scalar singlet DM scenario, we plot Fig. 2 to demonstrate the possibility to explain inflation and a

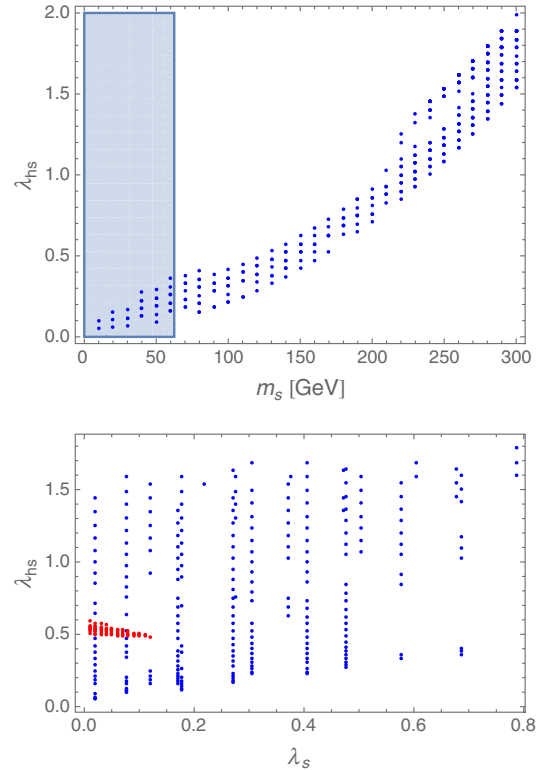


FIG. 2. Higgs-portal real scalar singlet DM scenario. In the red and blue dotted regions, we can obtain $h(s)$ inflation and a SFOEWPT. The blue region is excluded by the Higgs invisible decay bounds.

SFOEWPT. In the top and bottom panels, the shape of the two-step SFOEWPT allowed parameter spaces is mostly characterized by the requirement that the EW vacuum be a global vacuum at zero temperature, i.e., $V_0(h=0, s=\pm\sqrt{\mu_s^2/\lambda_s}) > V_0(h=v, s=0)$, which sets $\lambda_s > 2(m_s^2 - \lambda_{hs}v^2)/(m_h^2v^2)$, augmented by $\mu_s^2 = -(m_s^2 - \lambda_{hs}v^2/2) > 0$, which guarantee the existence of the local vacuum at $(h=0, s=\pm\sqrt{\mu_s^2/\lambda_s})$. In the two panels, the three free parameters m_s , λ_{hs} , and λ_s are chosen by considering the above requirements. In the phase transition process, the requirement that the vacuum in the direction of s appearing earlier than the one in the direction of h further constrains the parameter spaces. The Higgs invisible decay branching ratio excludes parameter spaces of $m_s < m_h/2$. The result is consistent with previous studies of the phase transition in the SM + 1 singlet model with Z_2 symmetry; see Refs. [43–45]. In that parameter space around the Higgs funnel regime, the explanation of DM is possible; see Ref. [32]. In the bottom plot, the DM mass is set to be $m_s \geq m_h/2$, considering the aforementioned Higgs invisible decay exclusion. The plot depicts that there is a chance to explain inflation in a small corner of the SFOEWPT allowed region. This is because the quartic scalar coupling λ_s is basically small as required by the perturbativity and unitarity at a high scale to realize slow-roll inflation. The relatively large λ_{hs} here shuts down the window to explain DM. It is different from the results of Ref. [46], in which the phase transition is estimated with the Coleman-Weinberg contributions being neglected and the T^2 terms of the high temperature expansion method being kept.

For the U(1) breaking complex scalar singlet model case, the DM mass is independent of the inflation dynamics since it does not enter into RGEs of quartic couplings. The effects of DM mass are negligible for the two-step EWPT process as studied previously in Refs. [28,29]. After taking into account the present Higgs data together with the electro-weak precision observables [41], we present the results with a benchmark of $\theta = 0.2$ in Fig. 3. The top panel shows that most of the parameter spaces are excluded by perturbativity and stability at the inflation scale, and only a small part of the SFOEWPT-favored parameter spaces allows the explanation of the slow-roll inflation, with the other part parameter spaces are excluded by perturbativity and stability at the inflation scale. The bottom panel shows that a larger v_s and smaller m_{h_2} are required to successfully implement cosmic inflation, in order to preserve the perturbativity of quartic coupling and make the vacuum stable up to the Planck scale. The critical temperature of the SFOEWPT is found to be $\mathcal{O}(10^2)$ GeV, which is larger than the freeze-out temperatures and consistent with the DM relic density computation. The magnitude of the relic density can increase from undersaturated to oversaturated with the increasing (decreasing) of v_s (m_{h_2}) since then one has a smaller DM-Higgs quartic coupling λ_{hs} [as indicated by Eq. (9)] and therefore a smaller annihilation cross section of dark matter pairs. The increasing (decreasing)

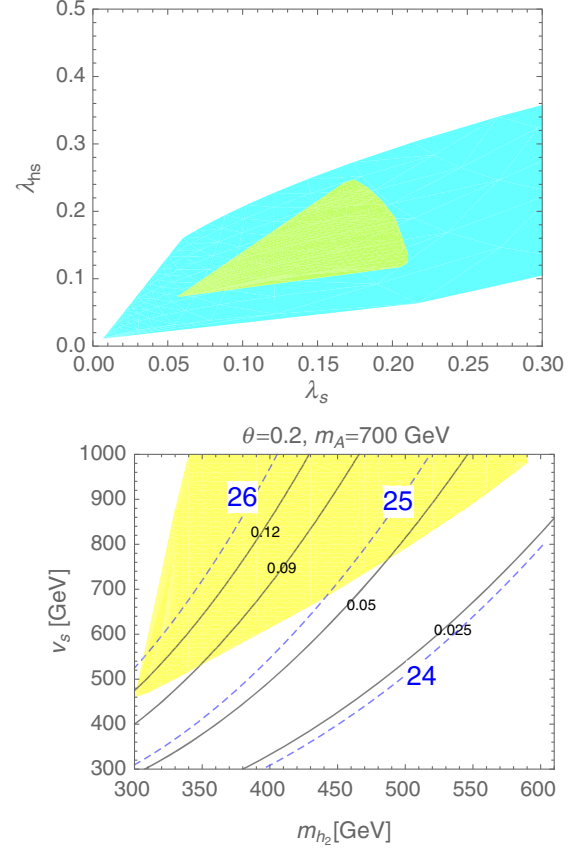


FIG. 3. U(1) breaking complex scalar singlet model for DM, inflation, and the SFOEWPT. The cyan and yellow regions are the successful SFOEWPT- and inflation-favored parameter spaces in the two plots. The freeze-out temperature is shown with the blue dashed line. The solid line represents the DM relic density, and the direct detection bounds from XENON1T yield null exclusions.

of dark matter mass m_A leads to oversaturation (undersaturation) of relic abundance in the successful inflation regions. One novel feature here is that the inflation, SFOEWPT, and DM explanation-favored parameter spaces do not suffer from the direct detection constraints even after the results of XENON1T [66] and future more stringent ongoing DM direct detection bounds, due to the cancellation effect of the DM-SM particle scattering amplitudes being explored in Ref. [38].

V. CONCLUSIONS AND DISCUSSIONS

In previous studies, two of the inflation, SFOEWPT, and DM have been explored in Higgs-portal models [42,45,46,59]. In this work, we investigate the possibility of accomplishing the three ingredients simultaneously in the framework of the usual Higgs-portal singlet scalar model and the complex singlet scalar model with the global U(1) being broken. For the Higgs-portal singlet scalar model, it is found that one cannot explain DM together with successful inflation and a two-step SFOEWPT. In comparison with the usual Higgs-portal singlet scalar dark

matter case, the DM direct detection bounds on parameter spaces in the scenario of the complex singlet scalar are vastly relaxed due to the two Higgs-mediated DM-SM particles scattering amplitude cancellation effects. In the scenario, we observe that a successful slow-roll inflation, a SFOEWPT, and the correct DM relic density can be accomplished after taking into account theoretical constraints, electroweak precision observables, and the present LHC Higgs data.

With an additional CP -violation source by implementing the CP Violation (CPV) dimension-6 operator [28], the flatness of the potential will not be destroyed, and the BAU can be generated during the EWPT process within the framework of EWBG. The search of the parameter spaces can be performed through the resonant heavy Higgs search at the LHC and Super proton-proton Collider (SppC) [25,41,67,68]. The gravitational wave signals generated during the EWPT with the typical spectrum frequency of $\mathcal{O}(10^{-4} - 10^{-2})$ Hz can also be used to test the parameter spaces. The physics picture in this work can be general and realized in many models supposing to some extent cancellation exists in the Higgs and other heavy Higgs-mediated DM-SM particles scattering processes.

ACKNOWLEDGMENTS

L. G. B. thanks Hyun Min Lee for helpful discussions on inflation. The work of L. G. B. is partially supported by the National Natural Science Foundation of China (under Grant No. 11605016); Basic Science Research Program, through the National Research Foundation of Korea funded by the Ministry of Education, Science and Technology (Grant No. NRF-2016R1A2B4008759); and Korea Research Fellowship Program through the National Research Foundation of Korea funded by the Ministry of Science and ICT (Grant No. 2017H1D3A1A01014046).

APPENDIX A: BETA FUNCTIONS

The one-loop beta functions for the various parameters can be found in the Higgs-portal real scalar singlet case [47], except that for the complex singlet scenarios, the scalar quartic coupling beta functions are replaced by

$$\beta_{\lambda_h} = \frac{3g_1^4}{128\pi^2} + \frac{3g_1^2g_2^2}{64\pi^2} - \frac{3g_1^2\lambda_h}{16\pi^2} + \frac{9g_2^4}{128\pi^2} - \frac{9g_2^2\lambda_h}{16\pi^2} - \frac{3g_t^4}{8\pi^2} + \frac{3g_t^2\lambda_h}{4\pi^2} + \frac{3\lambda_h^2}{2\pi^2} + \frac{\lambda_{hs}^2}{16\pi^2}, \quad (\text{A1})$$

$$\beta_{\lambda_s} = \frac{\lambda_{hs}^2}{8\pi^2} + \frac{5\lambda_s^2}{4\pi^2}, \quad (\text{A2})$$

$$\beta_{\lambda_{hs}} = -\frac{3g_1^2\lambda_{hs}}{32\pi^2} - \frac{9g_2^2\lambda_{hs}}{32\pi^2} + \frac{3g_t^2\lambda_{hs}}{8\pi^2} + \frac{3\lambda_h\lambda_{hs}}{4\pi^2} + \frac{\lambda_{hs}^2}{4\pi^2} + \frac{\lambda_{hs}\lambda_s}{2\pi^2}. \quad (\text{A3})$$

We use the electroweak-scale values of the various couplings consistent with Ref. [69] for the initial conditions of the RGEs.

APPENDIX B: FIELD-DEPENDENT MASSES AND THERMAL MASSES

The field-dependent masses are given by

$$M(h, s, A) = \begin{pmatrix} m_{hh} & m_{hs} & m_{hA} \\ m_{hs} & m_{ss} & m_{sA} \\ m_{hA} & m_{sA} & m_{AA} \end{pmatrix}, \quad (\text{B1})$$

with

$$m_{hh} = \frac{1}{2}(6\lambda_h h^2 - 2\mu_h^2 + \lambda_{hs}(s^2 + A^2)), \quad (\text{B2})$$

$$m_{hs} = \lambda_{hs}hs, \quad (\text{B3})$$

$$m_{hA} = \lambda_{hs}hA, \quad (\text{B4})$$

$$m_{ss} = \frac{1}{2}\lambda_{hs}h^2 - \mu_s^2 - \mu_b^2 + \lambda_s(3s^2 + A^2), \quad (\text{B5})$$

$$m_{sA} = 2\lambda_s sA, \quad (\text{B6})$$

$$m_{AA} = \frac{1}{2}\lambda_{hs}h^2 - \mu_s^2 + \mu_b^2 + \lambda_s(3A^2 + s^2). \quad (\text{B7})$$

The mass matrix (B1) can be diagonalized, with eigenvalues being $M_{1,2,3}^2$, and other field dependent masses are

$$M_{G^0}^2(h, s, A) = \frac{1}{2}(2\lambda_h h^2 + \lambda_{hs}A^2 - 2\mu_h^2 + \lambda_{hs}s^2), \quad (\text{B8})$$

$$M_{G^\pm}^2(h, s, A) = \frac{1}{2}(2\lambda_h h^2 + \lambda_{hs}A^2 - 2\mu_h^2 + \lambda_{hs}s^2), \quad (\text{B9})$$

$$M_I^2(h) = \frac{g_I^2 h^2}{2}, \quad (\text{B10})$$

$$M_Z^2(h) = \frac{1}{4}(g_1^2 + g_2^2)h^2, \quad (\text{B11})$$

$$M_W^2(h) = \frac{g_2^2 h^2}{4}. \quad (\text{B12})$$

The thermal masses/corrections in the U(1) breaking model are given by

$$M_{h_i}^2(T) = \frac{g_1^2 T^2}{16} + \frac{3g_2^2 T^2}{16} + \frac{g_t^2 T^2}{4} + \frac{\lambda_h T^2}{2} + \frac{\lambda_{hs} T^2}{12}, \quad (\text{B13})$$

$$M_{G^{0,\pm}}^2(T) = M_{h_i}^2(T), \quad (\text{B14})$$

$$M_s^2(T) = \frac{\lambda_{hs} T^2}{6} + \frac{\lambda_s T^2}{3}, \quad (\text{B15})$$

$$M_A^2(T) = \frac{\lambda_{hs} T^2}{6} + \frac{\lambda_s T^2}{3} \quad (\text{B16})$$

for the scalar fields; the gauge fields thermal masses can be found in Ref. [70].

APPENDIX C: DM ANNIHILATIONS CROSS SECTIONS

The relevant cubic and quartic interaction couplings are given by

$$\begin{aligned}
g_{h_1} &= \cos \theta, & g_{h_2} &= -\sin \theta, \\
g_{h_1 AA} &= \lambda_{hs} v \cos \theta + \lambda_s v_s \sin \theta, \\
g_{h_2 AA} &= 2\lambda_s v_s \cos \theta - \lambda_{hs} v \sin \theta, \\
g_{h_1 h_1 h_1} &= 3[2\lambda_h v (\cos \theta)^3 + \lambda_{hs} v (\sin \theta)^2 \cos \theta \\
&\quad + \lambda_{hs} v_s \sin \theta (\cos \theta)^2 + 2\lambda_s v_s (\sin \theta)^3], \\
g_{h_2 h_1 h_1} &= 2(\lambda_{hs} - 3\lambda_h) v \sin \theta (\cos \theta)^2 - \lambda_{hs} v (\sin \theta)^3 \\
&\quad + 2(3\lambda_s - \lambda_{hs}) v_s (\sin \theta)^2 \cos \theta + \lambda_{hs} v_s (\cos \theta)^3, \\
g_{h_2 h_2 h_2} &= 3(-2\lambda_h v (\sin \theta)^3 - \lambda_{hs} v \sin \theta (\cos \theta)^2 \\
&\quad + \lambda_{hs} v_s (\sin \theta)^2 \cos \theta + \lambda_s v_s (\cos \theta)^3), \\
g_{h_1 h_2 h_2} &= v(3\lambda_h - \lambda_{hs}) (\sin 2\theta) \sin \theta + \lambda_{hs} v (\cos \theta)^3 \\
&\quad + 2(3\lambda_s - \lambda_{hs}) v_s \sin \theta (\cos \theta)^2 + \lambda_{hs} v_s (\sin \theta)^3, \\
g_{h_1 h_2 AA} &= (2\lambda_s - \lambda_{hs}) \sin \theta \cos \theta, \\
g_{h_2 h_2 AA} &= \lambda_{hs} (\sin \theta)^2 + 2\lambda_s (\cos \theta)^2, \\
g_{h_1 h_1 AA} &= \lambda_{hs} (\cos \theta)^2 + 2\lambda_s (\sin \theta)^2. \tag{C1}
\end{aligned}$$

With these couplings and the propagators of $h_{1,2}$,

$$D_{h_1} = (4m_A^2 - m_{h_1}^2) + \Gamma_{h_1} m_{h_1}, \tag{C2}$$

$$D_{h_2} = (4m_A^2 - m_{h_2}^2) + \Gamma_{h_2} m_{h_2}, \tag{C3}$$

the thermal averaged annihilation cross sections are given by

$$\begin{aligned}
\langle \sigma v \rangle_{h_1 h_1} &= \frac{1}{64\pi m_A^2} \left| g_{AA h_1 h_1} + \frac{1}{D_{h_1}} g_{h_1 AA} g_{h_1 h_1 h_1} \right. \\
&\quad \left. + \frac{1}{D_{h_2}} g_{h_2 AA} g_{h_2 h_1 h_1} + \frac{2g_{h_1 AA}^2}{(m_{h_1}^2 - 2m_A^2)} \right|^2 \\
&\quad \times (1 - m_{h_1}^2/m_A^2)^{1/2}, \tag{C4}
\end{aligned}$$

$$\begin{aligned}
\langle \sigma v \rangle_{h_2 h_2} &= \frac{1}{64\pi m_A^2} \left| g_{AA h_2 h_2} + \frac{1}{D_{h_1}} g_{h_1 AA} g_{h_1 h_2 h_2} \right. \\
&\quad \left. + \frac{1}{D_{h_2}} g_{h_2 AA} g_{h_2 h_2 h_2} + \frac{2g_{h_2 AA}^2}{(m_{h_2}^2 - 2m_A^2)} \right|^2 \\
&\quad \times (1 - m_{h_2}^2/m_A^2)^{1/2}, \tag{C5}
\end{aligned}$$

$$\begin{aligned}
\langle \sigma v \rangle_{h_1 h_2} &= \frac{1}{32\pi m_A^2} \left| g_{AA h_1 h_2} + \frac{1}{D_{h_1}} g_{h_1 AA} g_{h_2 h_1 h_1} \right. \\
&\quad \left. + \frac{1}{D_{h_2}} g_{h_2 AA} g_{h_1 h_2 h_2} + \frac{g_{h_1 AA} g_{h_2 AA}}{(m_{h_1}^2 - 2m_A^2)} + \frac{g_{h_1 AA} g_{h_2 AA}}{(m_{h_2}^2 - 2m_A^2)} \right| \\
&\quad \times \sqrt{\left(1 + \frac{m_{h_1}^2 - m_{h_2}^2}{4m_A^2}\right) - \frac{m_{h_1}^2}{m_A^2}}, \tag{C6}
\end{aligned}$$

$$\begin{aligned}
\langle \sigma v \rangle_{h_1 h_2 bb} &= \frac{3m_W^2}{\pi g^2} \left(\frac{m_b}{v} \right)^2 \left| \frac{g_{h_1} (\lambda_{hs} g_{h_1} - \lambda_s g_{h_2})}{D_{h_1}} \right. \\
&\quad \left. + \frac{g_{h_2} (\lambda_{hs} g_{h_2} + \lambda_s g_{h_1})}{D_{h_2}} \right|^2 \left(1 - \frac{m_b^2}{M_A^2}\right)^{\frac{3}{2}}, \tag{C7}
\end{aligned}$$

$$\begin{aligned}
\langle \sigma v \rangle_{h_1 h_2 tt} &= \frac{3m_W^2}{\pi g^2} \left(\frac{m_t}{v} \right)^2 \left| \frac{g_{h_1} (\lambda_{hs} g_{h_1} - \lambda_s g_{h_2})}{D_{h_1}} \right. \\
&\quad \left. + \frac{g_{h_2} (\lambda_{hs} g_{h_2} + \lambda_s g_{h_1})}{D_{h_2}} \right|^2 \left(1 - \frac{m_t^2}{m_A^2}\right)^{\frac{3}{2}}, \tag{C8}
\end{aligned}$$

$$\begin{aligned}
\langle \sigma v \rangle_{h_1 h_2 WW} &= \frac{m_W^4}{8\pi m_A^2} \left| \frac{g_{h_1} (\lambda_{hs} g_{h_1} - \lambda_s g_{h_2})}{D_{h_1}} \right. \\
&\quad \left. + \frac{g_{h_2} (\lambda_{hs} g_{h_2} + \lambda_s g_{h_1})}{D_{h_2}} \right|^2 \\
&\quad \times \left(1 - \frac{m_W^2}{m_A^2}\right)^{\frac{1}{2}} \left(2 + \left(1 - 2\frac{m_A^2}{m_W^2}\right)^2\right), \tag{C9}
\end{aligned}$$

$$\begin{aligned}
\langle \sigma v \rangle_{h_1 h_2 ZZ} &= \frac{m_Z^4}{16\pi m_A^2} \left| \frac{g_{h_1} (\lambda_{hs} g_{h_1} - \lambda_s g_{h_2})}{D_{h_1}} \right. \\
&\quad \left. + \frac{g_{h_2} (\lambda_{hs} g_{h_2} + \lambda_s g_{h_1})}{D_{h_2}} \right|^2 \left(1 - \frac{m_Z^2}{m_A^2}\right)^{\frac{1}{2}} \\
&\quad \times \left(2 + \left(1 - 2\frac{m_A^2}{m_Z^2}\right)^2\right). \tag{C10}
\end{aligned}$$

- [1] A. H. Guth, *Phys. Rev. D* **23**, 347 (1981).
- [2] A. A. Starobinsky, *Phys. Lett.* **91B**, 99 (1980).
- [3] A. D. Linde, *Phys. Lett.* **108B**, 389 (1982).
- [4] P. A. R. Ade *et al.* (Planck Collaboration), *Astron. Astrophys.* **594**, A20 (2016).
- [5] G. Aad *et al.* (ATLAS Collaboration), *Phys. Lett. B* **716**, 1 (2012).
- [6] S. Chatrchyan *et al.* (CMS Collaboration), *Phys. Lett. B* **716**, 30 (2012).
- [7] F. L. Bezrukov and M. Shaposhnikov, *Phys. Lett. B* **659**, 703 (2008).
- [8] A. O. Barvinsky, A. Y. Kamenshchik, and A. A. Starobinsky, *J. Cosmol. Astropart. Phys.* **11** (2008) 021.
- [9] J. L. F. Barbon and J. R. Espinosa, *Phys. Rev. D* **79**, 081302 (2009).
- [10] A. O. Barvinsky, A. Y. Kamenshchik, C. Kiefer, A. A. Starobinsky, and C. F. Steinwachs, *Eur. Phys. J. C* **72**, 2219 (2012).
- [11] F. Bezrukov, A. Magnin, M. Shaposhnikov, and S. Sibiryakov, *J. High Energy Phys.* **01** (2011) 016.
- [12] C. P. Burgess, H. M. Lee, and M. Trott, *J. High Energy Phys.* **07** (2010) 007.
- [13] M. P. Hertzberg, *J. High Energy Phys.* **11** (2010) 023.
- [14] C. P. Burgess, H. M. Lee, and M. Trott, *J. High Energy Phys.* **09** (2009) 103.
- [15] X. Calmet and R. Casadio, *Phys. Lett. B* **734**, 17 (2014).
- [16] C. P. Burgess, S. P. Patil, and M. Trott, *J. High Energy Phys.* **06** (2014) 010.
- [17] F. Bezrukov, J. Rubio, and M. Shaposhnikov, *Phys. Rev. D* **92**, 083512 (2015).
- [18] J. Fumagalli and M. Postma, *J. High Energy Phys.* **05** (2016) 049.
- [19] V. M. Enckell, K. Enqvist, and S. Nurmi, *J. Cosmol. Astropart. Phys.* **07** (2016) 047.
- [20] G. Ballesteros, J. Redondo, A. Ringwald, and C. Tamarit, *Phys. Rev. Lett.* **118**, 071802 (2017).
- [21] R. N. Lerner and J. McDonald, *Phys. Rev. D* **83**, 123522 (2011).
- [22] A. D. Sakharov, *Pis'ma Zh. Eksp. Teor. Fiz.* **5**, 32 (1967) [*JETP Lett.* **5**, 24 (1967)]; *Usp. Fiz. Nauk* **161**, 61 (1991) [*Sov. Phys. Usp.* **34**, 392 (1991)].
- [23] D. E. Morrissey and M. J. Ramsey-Musolf, *New J. Phys.* **14**, 125003 (2012).
- [24] M. D'Onofrio, K. Rummukainen, and A. Tranberg, *Phys. Rev. Lett.* **113**, 141602 (2014).
- [25] N. Arkani-Hamed, T. Han, M. Mangano, and L. T. Wang, *Phys. Rep.* **652**, 1 (2016).
- [26] J. R. Espinosa, T. Konstandin, and F. Riva, *Nucl. Phys.* **B854**, 592 (2012).
- [27] S. Profumo, M. J. Ramsey-Musolf, C. L. Wainwright, and P. Winslow, *Phys. Rev. D* **91**, 035018 (2015).
- [28] M. Jiang, L. Bian, W. Huang, and J. Shu, *Phys. Rev. D* **93**, 065032 (2016).
- [29] C. W. Chiang, M. J. Ramsey-Musolf, and E. Senaha, *Phys. Rev. D* **97**, 015005 (2018).
- [30] B. Patt and F. Wilczek, [arXiv:hep-ph/0605188](https://arxiv.org/abs/hep-ph/0605188).
- [31] J. M. Cline and K. Kainulainen, *J. Cosmol. Astropart. Phys.* **01** (2013) 012.
- [32] J. M. Cline, K. Kainulainen, P. Scott, and C. Weniger, *Phys. Rev. D* **88**, 055025 (2013); *Phys. Rev. D* **92**, 039906(E) (2015).
- [33] M. Escudero, A. Berlin, D. Hooper, and M. X. Lin, *J. Cosmol. Astropart. Phys.* **12** (2016) 029.
- [34] V. Barger, M. McCaskey, and G. Shaughnessy, *Phys. Rev. D* **82**, 035019 (2010).
- [35] M. Gonderinger, Y. Li, H. Patel, and M. J. Ramsey-Musolf, *J. High Energy Phys.* **01** (2010) 053.
- [36] V. Barger, P. Langacker, M. McCaskey, M. Ramsey-Musolf, and G. Shaughnessy, *Phys. Rev. D* **79**, 015018 (2009).
- [37] M. Gonderinger, H. Lim, and M. J. Ramsey-Musolf, *Phys. Rev. D* **86**, 043511 (2012).
- [38] C. Gross, O. Lebedev, and T. Toma, *Phys. Rev. Lett.* **119**, 191801 (2017).
- [39] V. Barger, P. Langacker, M. McCaskey, M. J. Ramsey-Musolf, and G. Shaughnessy, *Phys. Rev. D* **77**, 035005 (2008).
- [40] M. Baak, J. Cúth, J. Haller, A. Hoecker, R. Kogler, K. Mönig, M. Schott, and J. Stelzer (Gitter Group Collaboration), *Eur. Phys. J. C* **74**, 3046 (2014).
- [41] M. Carena, Z. Liu, and M. Riembau, *Phys. Rev. D* **97**, 095032 (2018).
- [42] R. N. Lerner and J. McDonald, *Phys. Rev. D* **80**, 123507 (2009).
- [43] A. Beniwal, M. Lewicki, J. D. Wells, M. White, and A. G. Williams, *J. High Energy Phys.* **08** (2017) 108.
- [44] V. Vaskonen, *Phys. Rev. D* **95**, 123515 (2017).
- [45] D. Curtin, P. Meade, and C. T. Yu, *J. High Energy Phys.* **11** (2014) 127.
- [46] T. Tenkanen, K. Tuominen, and V. Vaskonen, *J. Cosmol. Astropart. Phys.* **09** (2016) 037.
- [47] A. Aravind, M. Xiao, and J. H. Yu, *Phys. Rev. D* **93**, 123513 (2016); **96**, 069901(E) (2017).
- [48] E. Elizalde and S. D. Odintsov, *Phys. Lett. B* **321**, 199 (1994).
- [49] E. Elizalde, S. D. Odintsov, E. O. Pozdeeva, and S. Y. Vernov, *Phys. Rev. D* **90**, 084001 (2014).
- [50] F. Kahlhoefer and J. McDonald, *J. Cosmol. Astropart. Phys.* **11** (2015) 015.
- [51] F. Bezrukov, D. Gorbunov, and M. Shaposhnikov, *J. Cosmol. Astropart. Phys.* **06** (2009) 029.
- [52] L. Dolan and R. Jackiw, *Phys. Rev. D* **9**, 3320 (1974).
- [53] H. H. Patel and M. J. Ramsey-Musolf, *J. High Energy Phys.* **07** (2011) 029.
- [54] P. B. Arnold and O. Espinosa, *Phys. Rev. D* **47**, 3546 (1993); **50**, 6662(E) (1994).
- [55] J. Bernon, L. Bian, and Y. Jiang, *J. High Energy Phys.* **05** (2018) 151.
- [56] G. W. Anderson and L. J. Hall, *Phys. Rev. D* **45**, 2685 (1992).
- [57] M. E. Carrington, *Phys. Rev. D* **45**, 2933 (1992).
- [58] J. M. Cline, K. Kainulainen, and D. Tucker-Smith, *Phys. Rev. D* **95**, 115006 (2017).
- [59] W. Chao, *Phys. Rev. D* **92**, 015025 (2015).
- [60] J. McDonald, *Phys. Rev. D* **50**, 3637 (1994).

- [61] O. Catà, A. Ibarra, and S. Inghütt, *Phys. Rev. D* **95**, 035011 (2017).
- [62] O. Catà, A. Ibarra, and S. Inghütt, *Phys. Rev. Lett.* **117**, 021302 (2016).
- [63] E. W. Kolb and M. S. Turner, *The Early Universe* (Addison-Wesley, Reading, MA, 1990).
- [64] <https://laph.cnr.fr/micromegas/>.
- [65] P. A. R. Ade *et al.* (Planck Collaboration), *Astron. Astrophys.* **594**, A13 (2016).
- [66] E. Aprile *et al.* (XENON Collaboration), *Phys. Rev. Lett.* **119**, 181301 (2017).
- [67] A. V. Kotwal, M. J. Ramsey-Musolf, J. M. No, and P. Winslow, *Phys. Rev. D* **94**, 035022 (2016).
- [68] T. Huang, J. M. No, L. Pernié, M. Ramsey-Musolf, A. Safonov, M. Spannowsky, and P. Winslow, *Phys. Rev. D* **96**, 035007 (2017).
- [69] D. Buttazzo, G. Degrassi, P. P. Giardino, G. F. Giudice, F. Sala, A. Salvio, and A. Strumia, *J. High Energy Phys.* **12** (2013) 089.
- [70] R. G. Cai, M. Sasaki, and S. J. Wang, *J. Cosmol. Astropart. Phys.* **08** (2017) 004.